arXiv:1508.02093v1 [cond-mat.mes-hall] 9 Aug 2015

Dynamic detection of electron spin accumulation in ferromagnet-semiconductor devices by ferromagnetic resonance

Changjiang Liu,[1] Sahil J. Patel,[2] Timothy A. Peterson,[1] Chad C. Geppert,[1]
Kevin D. Christie,[1] Gordon Stecklein,[1] Chris J. Palmstrøm,[2,3] and Paul A. Crowell[1,*]

[1]*School of Physics and Astronomy, University of Minnesota, Minneapolis, Minnesota 55455, USA*

[2]*Department of Materials, University of California, Santa Barbara, California 93106, USA*

[3]*Department of Electrical and Computer Engineering, University of California, Santa Barbara, California 93106, USA*

Abstract

A distinguishing feature of spin accumulation in ferromagnet-semiconductor devices is precession of the non-equilibrium spin population of the semiconductor in a magnetic field. This is the basis for detection techniques such as the Hanle effect, but these approaches become less effective as the spin lifetime in the semiconductor decreases. For this reason, no electrical Hanle measurement has been demonstrated in GaAs at room temperature. We show here that by forcing the magnetization in the ferromagnet (the spin injector and detector) to precess at the ferromagnetic resonance frequency, an electrically generated spin accumulation can be detected from 30 to 300 K. At low temperatures, the distinct Larmor precession of the spin accumulation in the semiconductor can be detected by ferromagnetic resonance in an oblique field. We verify the effectiveness of this new spin detection technique by comparing the injection bias and temperature dependence of the measured spin signal to the results obtained using traditional methods. We further show that this new approach enables a measurement of short spin lifetimes (< 100 psec), a regime that is not accessible in semiconductors using traditional Hanle techniques.

* crowell@umn.edu

An effective means to electrically detect electron spin accumulation in a semiconductor is essential to the development of semiconductor spintronics[1,2]. A common detection method, known as the Hanle effect[3], relies on the precession of the spin accumulation in the semiconductor by an external magnetic field. This approach has been employed in both the non-local[4,5] and the local 3-terminal (3T)[6] measurement geometries. As the spin lifetime decreases at higher temperatures, a significantly higher magnetic field is required in order for the Hanle effect to dephase the spin accumulation[7]. The ordinary magnetoresistance in semiconductors in such large fields produces large quadratic backgrounds[6] that mask any truly spin-dependent effects. As a result, no electrical Hanle measurement has been demonstrated in *n*-GaAs at room temperature. Although the 3T technique has recently been widely used to study spin transport in new material systems[8–10] at higher temperatures, it has been shown that the 3T Hanle measurement is sensitive to a variety of magnetic field assisted phenomena[11–13], which often cannot be separated from the Hanle effect.

We introduce here a new detection technique, which utilizes the precession of the magnetization under ferromagnetic resonance (FMR) to dynamically detect the spin accumulation in a semiconductor. The approach is similar in some aspects to a Hanle measurement, in that the observed signal corresponds to a suppression of the component of the spin accumulation parallel to the magnetization. In this case, however, the suppression is due to the onset of FMR rather than precession of the spin accumulation in an orthogonal magnetic field. The narrow FMR linewidth and the sensitivity to both the precession of the magnetization in the ferromagnet as well as the dynamics of the spin accumulation in the semiconductor provide an immunity to the field-dependent backgrounds that affect Hanle measurements, particularly in the 3T case. At low temperatures, the Larmor precession of the spin accumulation in the semiconductor can be detected by an FMR measurement in an oblique magnetic field. We verify the effectiveness of this approach by comparing the bias and temperature dependence of the measured spin signal to results obtained on the same heterostructures using traditional spin detection methods. Finally, we show that this FMR-based spin detection technique enables one to determine the spin relaxation rate in GaAs at room temperature, at which an ordinary Hanle curve cannot be measured.

The devices used in this electrical spin injection and detection experiment consist of ferromagnet (FM)/semiconductor (SC) heterostructures. A spin current across the FM/SC interface is generated by a current source[14,15], leading to a spin accumulation, which has previously been detected potentiometrically[5,16] or by using a spin filter to detect the polarized current[17]. In the potentiometric approach, the voltage detected by a FM contact due to spin accumulation can be

expressed as[5]

$$V = \eta P_{\mathrm{FM}} \frac{1}{e} \frac{\partial \mu}{\partial n} \mathbf{s} \cdot \hat{\mathbf{m}}, \tag{1}$$

where η is the spin detection efficiency, P_{FM} is the spin polarization at the Fermi level in the FM, e is the electron charge, and μ and n are the chemical potential and number density of electrons in the SC. The spin accumulation $\mathbf{s}$ in the SC has a magnitude defined as $|\mathbf{s}| = n_{\uparrow} - n_{\downarrow}$, where $n_{\uparrow}$ and $n_{\downarrow}$ refer to the number density of spin-up and spin-down electrons, and $\hat{\mathbf{m}}$ is the unit vector of the magnetization $\mathbf{m}$ in the FM. The dot product in equation (1) accounts for the projection of the spin accumulation, which must be averaged over the area of the contact, onto the magnetization. In a Hanle measurement, one applies a magnetic field perpendicular to $\hat{\mathbf{m}}$ to precess and dephase the injected spins, thus reducing the magnitude and changing the orientation of $\mathbf{s}$. In our experiment, we force the magnetization of the FM to precess instead of the spin accumulation in the SC. We inject spins from the FM and simultaneously drive the magnetization in the FM to precess by FMR. During this process, $\mathbf{s} \cdot \hat{\mathbf{m}}$ also changes, which allows for detection of the spin accumulation. As will be explained in detail in the modeling section, the important time scales in this experiment are the FMR precession period and the electron spin lifetime τ_s in the SC. Together these determine the steady state value of $\mathbf{s} \cdot \hat{\mathbf{m}}$, which changes at resonance.

Results

Experimental setup and room temperature measurement. Figure 1a is a schematic diagram of the FMR-spin detection experiment. The devices used in our experiment are fabricated from epitaxial FM/n-GaAs (100) heterostructures. Recently, the utilization of the ferromagnetic Heusler alloys[19] has greatly improved the spin injection efficiency into GaAs[20,21]. In our experiment, we use the Heusler alloys Co_2MnSi and Co_2FeSi as spin injectors. The FM film is 5 nm thick with lateral dimensions of 5×50 μm. The n-GaAs is doped with a concentration of $n = 3 \times 10^{16}$ cm^{-3}. The junction region consists of a highly doped $n^{+}(5 \times 10^{18}$ cm$^{-3})$ layer to thin the Schottky tunnel barrier in order to achieve higher spin injection efficiency[22,23]. A 120 nm thick gold wire, which forms a microwave stripline, is deposited directly on top of the FM contact. The microwave Oersted field from the stripline drives the resonance. The microwave frequency used in the experiment ranges from 5 Ghz to 20 Ghz. The applied dc magnetic field is in the sample plane as indicated by $\mathbf{H}$ in Fig. 1a. A forward bias current across the FM/SC interface injects a spin current into the n-GaAs[24]. The microwave field is modulated at low frequency (100 Hz) and a lock-in amplifier synchronized with the modulation frequency measures the difference in interface voltage with

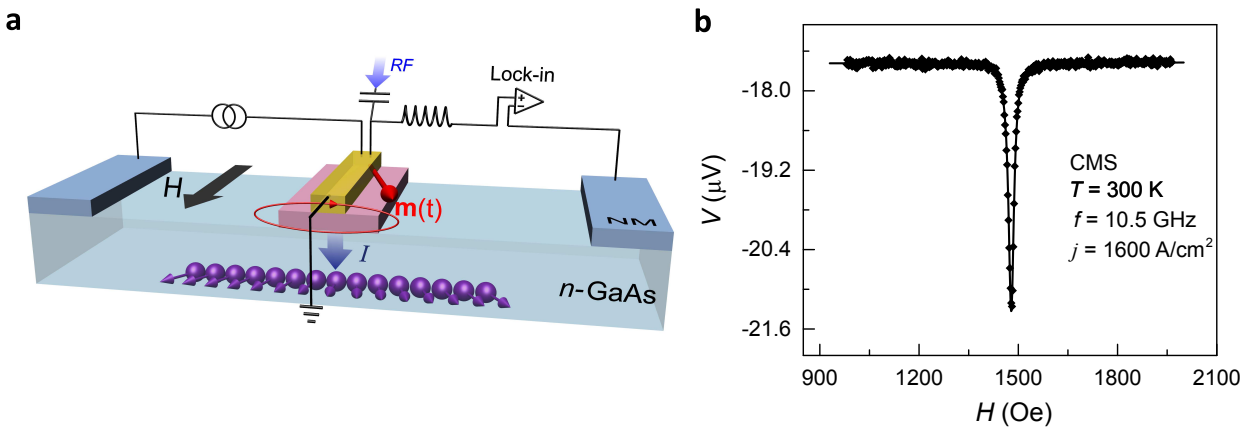

Figure 1. **Schematic diagram of the experiment and a representative plot of the spin accumulation data measured by FMR at room temperature.** (**a**) A schematic diagram of the FMR-spin detection experiment. The red contact in the middle of the device is ferromagnetic. On top of the ferromagnet is the microwave stripline (shown in yellow). The two remote contacts (shown in blue) are ohmic and are fabricated from non-magnetic Cu-Ge[18]. **H** and **m**(t) represent the applied magnetic field and the precessing magnetization of the FM, respectively. I is the applied interface bias current, which generates a spin accumulation in n-GaAs. Spins (shown in purple) injected by the precessing magnetization at different times have different orientations, and they diffuse in the n-GaAs channel. (**b**) Spin signal measured by FMR as a decrease in voltage at room temperature. The solid line is a Lorentzian fit to the data. CMS refers to the sample with Co_2MnSi as the FM.

microwaves on and off.

When the bias current generates a spin accumulation in the n-GaAs and the magnetization is driven on resonance, a dip in the three-terminal voltage is observed. The raw data in Figure 1b show the resonance observed at room temperature. The resonance field measured as a function of the microwave frequency agrees with the FMR spectrum as calculated from Kittel's formula[25] using the anisotropy and magnetization of each sample (see Supplementary Fig. 1). The non-zero background voltage in the plot is due to the nonlinear IV characteristic of the FM/n-GaAs Schottky contact[26], which rectifies the microwave current generated in the device. We see that the interface voltage decreases on resonance, which, as will be explained in detail below, is the result of the decrease of the projection of **s** onto $\hat{\mathbf{m}}$. In previous work, we found that the tunneling anisotropic magnetoresistance (TAMR) effect at the FM/SC interface also produces a change in the interface voltage at FMR[27]. The size of the TAMR effect depends on the bias voltage across

the FM/SC interface[27,28]. When a high forward bias current is applied to the sample generating a spin accumulation in the SC, the FMR signal due to the TAMR effect is much smaller than that produced by the spin accumulation[27]. In the data analysis below, the small contribution to the FMR signal from the TAMR effect has been removed.

Detecting the Larmor precession. A distinguishing feature of spin is the Larmor precession about an applied magnetic field. The precession frequency is $\omega_L = g\mu_B B/\hbar$, where μ_B is the Bohr magneton, the g factor is -0.44 for electrons in GaAs[29] and $\hbar$ is Planck's constant. We expect that the Larmor precession in the SC will influence the spin accumulation measured by FMR when ω_L is larger than the spin relaxation rate. In these samples, this condition can be achieved at low temperatures (30 K), at which the spin lifetime for this doping is longer than 10 ns[30], while the the Larmor precession period is about 1 ns for a magnetic field of 2000 Oe. We tilt the magnetic field out of the sample plane such that the perpendicular component of the magnetic field is still much smaller than the magnetic anisotropy field of the FM film. This allows the magnetization to remain nearly in the sample plane, while the spins in the semiconductor precess about the oblique magnetic field. In steady state, the spin accumulation can be viewed as an ensemble of spins injected at different times[3]. When $\omega_L > \tau_s^{-1}$, as is the case at 30 K, the orientations of electron spins are therefore distributed uniformly on the precession cone, which is depicted in purple in Fig. 2b. In other words, the *transverse* component of the spin accumulation is completely dephased, and there is no component of the steady-state spin accumulation perpendicular to the applied field.

Figure 2a shows that the FMR spin accumulation signal decreases significantly as the out-of-plane angle θ of the magnetic field increases. To verify that this change is not simply due to the magnetization dynamics of the FM, we confirm that the amplitude of the precession cone angle in the FM does not change significantly with increasing angle by applying a *reverse* bias across the FM/*n*-GaAs interface. Under reverse bias, there is no spin accumulation generated in the *n*-GaAs, as we have verified in traditional non-local spin valve measurements, and the interface voltage at resonance is due only to the TAMR. The TAMR can in turn be related very simply to the geometry of the precessing magnetization in the FM (see Supplementary Note 2). Figure 2c shows almost no change in the size of the voltage peak when the field is tilted out of plane, and hence we conclude that the amplitude of the precession cone angle in the FM is nearly constant.

The spin accumulation detected by the FM is proportional to $\langle \mathbf{s} \cdot \hat{\mathbf{m}} \rangle$, where the brackets indicate the time average in steady state. Because the transverse spin is completely dephased under the

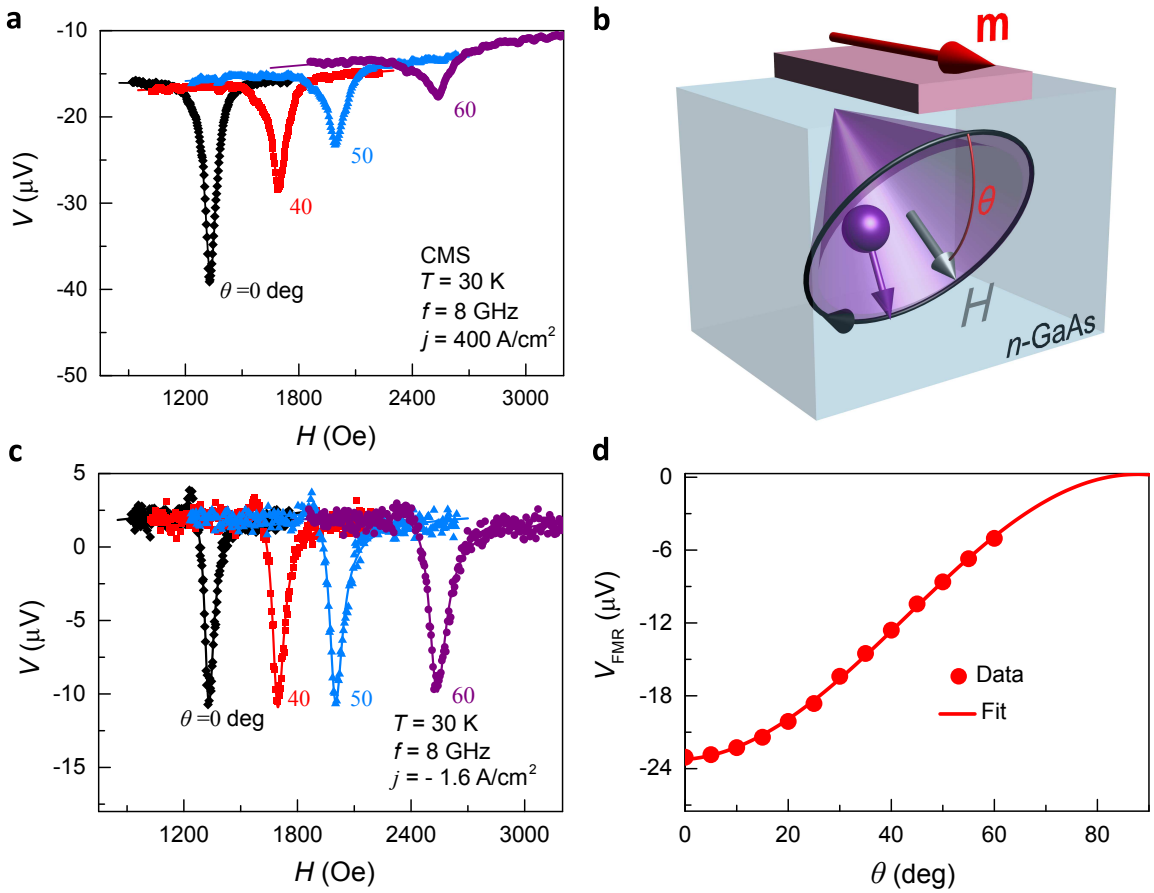

Figure 2. Experimental results in the oblique configuration at 30 K and illustration of the Larmor precession of the spin accumulation. (**a**) The FMR signal measured at different out-of-plane angles of the applied field when a spin accumulation exists in the *n*-GaAs. Note the decrease in the signal amplitude with increasing angle. (**b**) The applied magnetic field **H**, represented by the grey arrow, is tilted out-of-plane by an angle θ. The injected spins precess about **H** and their directions are uniformly distributed on a cone when $\tau_s \gg \frac{2\pi}{\omega_L}$, as is the case at 30 K. (**c**) FMR measured under reverse bias, at which only the TAMR effect is present. The out-of-plane angles are the same as in Fig. 2a. In this case the amplitude is independent of angle. (**d**) Angle dependence of the magnitude of the spin accumulation signal measured by FMR (Fig. 2a), and a fit based on the Larmor precession model. Because of the large demagnetizing field, the precession axis of the magnetization remains nearly in the sample plane. The raw data in (**a**,**c**) are plotted as a function of the total magnetic field, and so the resonance field positions and the widths of the peaks scale as $1/\cos\theta$ relative to the in-plane ($\theta = 0$) case.

conditions being considered, the *magnitude* of the spin accumulation is reduced by a factor of $\cos\theta$ relative to its magnitude s_0 when the field is in the sample plane. As a result, $\mathbf{s} = s_0 \cos\theta \hat{\mathbf{h}}$,

where $\hat{\mathbf{h}}$ is a unit vector parallel to the magnetic field. Because the detected voltage is proportional to $\langle \mathbf{s} \cdot \hat{\mathbf{m}} \rangle$ and none of the prefactors in equation (1) depend on angle, the spin accumulation signal at resonance should therefore vary as $\cos^2\theta$. Figure 2d shows the amplitude of the resonant signal V_{FMR} (the magnitudes of the negative peaks in Fig. 2a) as a function of θ. The solid line is a fit to $\cos^2\theta$, and so the behavior expected for a spin accumulation signal is observed.

Comparison to other measurement techniques. To obtain further evidence that the observed FMR signal is due to the spin accumulation in the *n*-GaAs layer, we measure the dependence of V_{FMR} on the bias current and temperature. The resulting data can then be compared to those obtained using other techniques. We first use the 3T Hanle measurement, carried out in a perpendicular field, to measure the spin accumulation at different injection bias currents[6,31]. Figure 3a shows the measured 3T signal V_{3T} at 30 K for different forward bias currents, and Fig. 3b shows V_{3T} at a fixed forward bias current for different temperatures. The asymmetric lineshape and the narrowing of the peak at low magnetic field in Fig. 3a are caused by the hyperfine interaction between the injected spins and the polarized nuclei[32]. At low temperature, V_{3T} is nearly proportional to the spin accumulation[6], and so we expect the bias dependences of V_{3T} and V_{FMR} to be the same. In Fig. 3c, V_{3T} and the FMR signal at 30 K are plotted as a function of the bias voltage. The two measurement techniques agree up to a single bias-independent scale factor. Unfortunately, this comparison cannot be made at high temperatures, at which a spin-dependent contribution to V_{3T} cannot be measured, as can be seen from the 300 K data in Fig. 3b. We have also performed non-local Hanle measurements[5] on this sample (see Supplementary Fig. 2) . Although consistent with V_{3T} up to 120 K, the non-local Hanle signal also cannot be measured at higher temperatures.

The steady-state spin accumulation in the semiconductor depends on the spin lifetime and diffusion constant[7], which are strong functions of temperature. The Hanle techniques fail at high temperatures because the magnetic field scale corresponding to $\omega_L \tau_s \sim 1$ grows dramatically as τ_s decreases. As a result, the Hanle curves broaden and cannot be distinguished from field-dependent backgrounds. This limitation does not impact the FMR signal, as we can see by comparison with non-local spin valve measurements[5]. Spin valves with source-detector separations between 250 nm and 2 μm were fabricated for each heterostructure by electron beam lithography. In this case, the field is swept in the plane, and the spin accumulation is inferred from the magnitude of the jump V_{NLSV} in the voltage when the source and detector magnetizations switch from parallel to antiparallel. Data for Co_2FeSi/n-GaAs at a source-detector separation of 250 nm are shown in Fig. 3d. This spacing is smaller than the spin diffusion length of approximately 800 nm at room

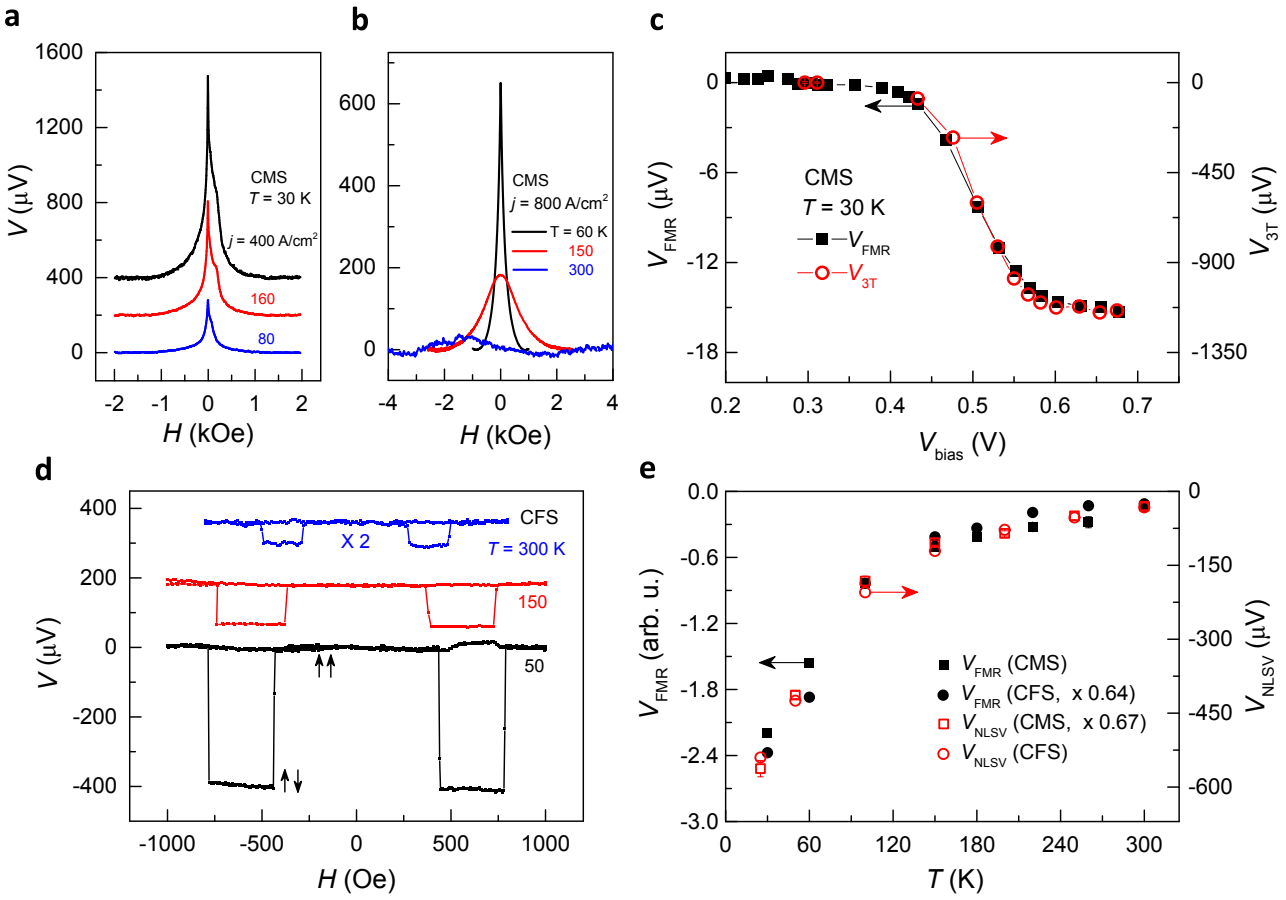

Figure 3. **Injection bias and temperature dependence of the spin accumulation measured by traditional methods and their comparison to the results obtained by the FMR technique.** (**a**) 3T data measured as a function of perpendicular field at 30 K for different injection bias currents. (**b**) 3T signal measured at different temperatures for a fixed bias current. The spin signal cannot be resolved using the Hanle measurement at 300 K. (**c**) Magnitude of the FMR peak, V_{FMR} (black squares, left axis), and V_{3T} (red circles, right axis) plotted as a function of injection bias voltage at 30 K. Note that the two sets of measurements differ by only a single bias-independent scale factor. (**d**) Non-local spin valve measurements at different temperatures, obtained at a source-detector separation of 250 nm. The 300 K data are multiplied by a factor of 2 for clarity. The arrows indicate the relative orientations of the magnetization in the source and detector FM. In **a**, **b** and **d** a second order background has been subtracted from the raw data. Curves in **a** and **d** are offset for clarity. (**e**) V_{FMR} (black solid symbols, left axis) and V_{NLSV} (red open symbols, right axis) measured as a function of temperature. CMS and CFS refer to samples with Co_2MnSi and Co_2FeSi as the FM, respectively.

temperature (see Supplementary Fig. 4), and so it is possible to measure V_{NLSV} over the entire

temperature range of this experiment. Figure 3e compares V_{FMR} with V_{NLSV} for both Co_2FeSi/n-GaAs and Co_2MnSi/n-GaAs from 30 K to 300 K. The temperature dependences are similar for both sets of measurements on each heterostructure. Note that the choice of FM should not matter in this case, as the temperature dependence is governed primarily by properties of the SC.

Modeling and measuring the frequency dependence to study spin relaxation. The data of Fig. 3 demonstrate that V_{FMR} is proportional to the spin accumulation. We now consider the frequency dependence of V_{FMR} and its relationship to τ_s. Remarkably, we find that the FMR technique can provide a measurement of the spin lifetime in the regime $\omega_{\mathrm{FMR}}\tau_s \sim 1$, which turns out to be accessible at *high* temperatures. In this limit, a spin injected from the FM relaxes before the magnetization precesses through a complete cycle. This physical scenario is illustrated in Fig. 4a, in which the spin accumulation is represented by a series of spins (in purple) that have been injected into the semiconductor at the times indicated, where t_0 corresponds to the present, and $-t_3$ through $-t_1$ represent *previous* times as labeled on the trajectory of the precessing magnetization, which is shown in red. The spins shown are oriented approximately parallel to the magnetization at the time at which those spins were injected. Precession in the semiconductor is ignored because $\omega_L < \omega_{\mathrm{FMR}}/10$ for the entire frequency and magnetic field range covered by the experiment. The smaller number of spins present from the earlier times is due to the relaxation of spins over time. The average spin accumulation, shown by the large purple arrow in Fig. 4a, is therefore a vector which lags behind the precessing magnetization.

The spin accumulation signal under these conditions can be calculated by an appropriately weighted time average of equation (1), incorporating spin relaxation and diffusion[6]:

$$V(t) = \eta P_{\mathrm{FM}} \frac{j_s}{e}\frac{\partial \mu}{\partial n}\int_{-\infty}^{\mathrm{t}} \frac{\hat{\mathbf{m}}(t)\cdot\hat{\mathbf{s}}(t')}{\sqrt{2\pi D(t-t')}}\exp[-\frac{t-t'}{\tau_s}]dt', \qquad (2)$$

where j_s is the injected spin current density, while D and τ_s are the spin diffusion constant and the spin lifetime in n-GaAs. Here $\hat{\mathbf{m}}(t)$ and $\hat{\mathbf{s}}(t')$ represent the time-dependent orientations of the magnetization and the injected spins, respectively. The integral over t' evaluates the projection of the spins injected at all previous times, reduced by the effects of diffusion and relaxation, onto the present magnetization direction $\hat{\mathbf{m}}(t)$. This is the *instantaneous* voltage detected by the FM. In the FM thin film, the precessing magnetization traces out an ellipse, with an in-plane cone angle φ_{in} and an out-of-plane angle φ_{out}. From geometric analysis (ignoring the Larmor precession in the SC as noted in the previous paragraph), $\hat{\mathbf{m}}(t)\cdot\hat{\mathbf{s}}(t')$ takes the form

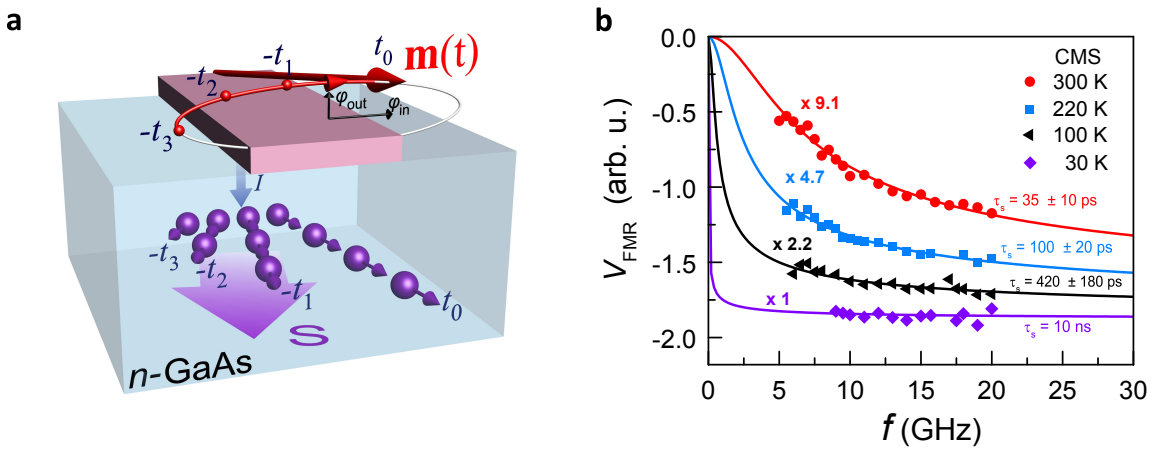

Figure 4. **Illustration of the spin accumulation in the short spin lifetime regime and the frequency dependence of V_{FMR} at different temperatures.** (**a**) Injected spins (small purple arrows in *n*-GaAs) are parallel to the instantaneous orientation of the magnetization (red arrow on top of the FM) at the time they are injected. Earlier injected spins, e.g., at $t = -t_1$, $-t_2$ or $-t_3$ have progressively smaller magnitudes due to spin relaxation and diffusion. The orientation of the average spin accumulation, indicated by the large purple vector **S**, lags behind the magnetization **m**, which decreases $\mathbf{s}\cdot\hat{\mathbf{m}}$ relative to the static case ($\omega = 0$). (**b**) V_{FMR} measured as a function of frequency at different temperatures. For clarity, signal sizes are multiplied by the factors shown in the plot. The solid lines are fits based on equation (4) derived in the main text, from which the electron spin lifetime in the SC is obtained. For the 30 K data, the solid line is calculated from the expression of $V_{\mathrm{FMR}}(\omega)$ by using the known spin lifetime $\tau_s = 10$ ns.

$$\hat{\mathbf{m}}(t)\cdot\hat{\mathbf{s}}(t') = 1 - \frac{\varphi_{\mathrm{in}}^2}{2}(\cos\omega t - \cos\omega t')^2 - \frac{\varphi_{\mathrm{out}}^2}{2}(\sin\omega t - \sin\omega t')^2, \tag{3}$$

(see Supplementary Note 3), in which ω is precession frequency in the FM. The dc voltage $\langle V(t)\rangle$ in the presence of a microwave field is the average value of $V(t)$ over a precession period. The magnitude of $V_{\mathrm{FMR}}(\omega)$ is the difference of $\langle V(t)\rangle$ between resonance ($\omega = \omega_{\mathrm{FMR}}$) and off resonance, which can be determined by setting $\omega = 0$ in equation (2). We then obtain

$$V_{\mathrm{FMR}}(\omega) = \frac{1}{2}\eta P_{\mathrm{FM}}\frac{j_s}{eN(E_{\mathrm{f}})}(\varphi_{\mathrm{in}}^2 + \varphi_{\mathrm{out}}^2)\sqrt{\frac{\tau_s}{2D}} \times \left(\sqrt{\frac{1}{2\sqrt{1+\omega^2\tau_s^2}} + \frac{1}{2(1+\omega^2\tau_s^2)}} - 1\right). \tag{4}$$

From equation (4) we obtain $\lim_{\omega\to 0} V_{\mathrm{FMR}}(\omega) = 0$. This corresponds to the dc limit, in which the orientation of the spin accumulation is always able to follow the magnetization. As ω increases,

the angle by which the spin accumulation "lags" the magnetization increases, and $V_{\mathrm{FMR}}(\omega)$ becomes more negative. The expression for $V_{\mathrm{FMR}}(\omega)$ suggests that in the regime $\omega\tau_s \sim 1$, $V_{\mathrm{FMR}}(\omega)$ will have considerable frequency dependence. This regime corresponds to short spin lifetimes, ie., $\tau_s \sim 16$ ps for a typical FMR frequency of $f = \omega/2\pi = 10$ GHz. As ω increases further, $V_{\mathrm{FMR}}(\omega) \rightarrow -\frac{1}{2}\eta P_{\mathrm{FM}} \frac{j_s}{eN(E_{\mathrm{f}})}(\varphi_{\mathrm{in}}^2 + \varphi_{\mathrm{out}}^2)\sqrt{\frac{\tau_s}{2D}}$ and saturates (no frequency dependence). This situation is equivalent to the long τ_s limit which happens at low temperature. We note that the magnitude of $V_{\mathrm{FMR}}(\omega)$ in this case is proportional to the steady-state spin accumulation, with the proportionality determined by the magnitude of the precession cone angles. This explains the data presented in Figs 2 and 3.

To test this model, we measure the frequency dependence of V_{FMR} at different temperatures. During the measurement, the injection bias current is fixed, and the amplitude of the magnetization precession, which is measured from the TAMR at reverse bias[27], is fixed at a constant value by adjusting the microwave power at each frequency. Figure 4b presents the experimental results. The FMR signal shows a pronounced frequency dependence at high temperatures. The magnitude of the signal increases as the FMR frequency increases, and the sign of the effect is negative as expected from the decrease in $\langle \mathbf{s} \cdot \hat{\mathbf{m}} \rangle$. The solid lines in Fig. 4b are fits to $V_{\mathrm{FMR}}(\omega)$ given by equation (4), except for the 30 K data, for which τ_s is fixed at the value (10 nsec) inferred from non-local spin valve measurements. Besides an overall scale factor, the spin lifetime τ_s is the only fitting parameter (D is absorbed into the prefactor in equation (4)). We obtain a spin lifetime of $\tau_s = 35 \pm 10$ ps in *n*-GaAs at room temperature. This value is comparable to previous theoretical calculations based on D'yakonov and Perel' (DP) spin relaxation in bulk GaAs[33] as well as the value of τ_S (50 ± 10 ps) extracted from non-local spin valve measurements (see Supplementary Fig. 4). The frequency dependence in Fig. 4b disappears as the temperature is lowered to 30 K. In this limit, the magnetization precesses through multiple cycles before the spin accumulation relaxes, and V_{FMR} should therefore be insensitive to frequency, as is found experimentally.

Discussion

In summary, we have demonstrated a new technique based on FMR to measure spin accumulation in ferromagnet-semiconductor devices. The precession of the magnetization at resonance leads to a measurable phase lag between the spin accumulation in the SC and the magnetization in the FM. Because the voltage detected by the FM is proportional to the projection of the spin accumulation onto the magnetization, the spin accumulation voltage decreases at resonance. The typical FMR

frequency is larger than the spin relaxation rate, and so the spin accumulation can be measured up to room temperature, making this approach more effective than the traditional Hanle effect, which has previously limited spin lifetime measurements in GaAs-based spin transport devices to temperatures less than approximately 150 K. FMR occurs within a narrow magnetic field window, and the spin accumulation signal detected by the FM is sensitive to the precession of the magnetization. Together these make the technique essentially immune to the field-dependent backgrounds that plague Hanle measurements, particularly at high temperatures. By measuring the frequency dependence of the spin accumulation signal, spin relaxation in the SC can be probed directly. With this method, we obtain an electron spin lifetime of a few tens of picoseconds in *n*-GaAs ($n = 3 \times 10^{16}\text{cm}^{-3}$) at room temperature. The FMR-based spin detection technique developed here can be used above room temperature and applied to other material systems, such as metals, in which the spin lifetimes are short and traditional Hanle measurements are impractical.

Methods

Sample growth. The FM/*n*-GaAs heterostructures investigated in this experiment were grown by molecular beam epitaxy on GaAs (001) substrates. The growth started with a 500 nm undoped GaAs buffer layer, followed by 2500 nm of Si-doped *n*-GaAs ($n = 3\times10^{16}\text{cm}^{-3}$). The junction region consists of a 15 nm $n \rightarrow n^+$-GaAs transition layer followed by 18 nm $n^+(5\times10^{18}\text{cm}^{-3})$ GaAs[5]. The 5 nm thick FM film was then deposited epitaxially, followed by 10 nm thick Al and Au capping layers. The deposition temperatures for Co_2MnSi and Co_2FeSi were 220°C and 270°C, respectively.

Device fabrication. Ion milling was used to define the 5 μm $\times$ 50 μm FM contacts. The remote 50 μm $\times$ 50 μm non-magnetic contacts were fabricated by depositing 40 nm Cu and then 40 nm Ge using electron beam evaporation. The CuGe contacts were prepared in pairs and annealed by passing a current through them in order to make them ohmic. This step avoids thermal annealing of the FM/*n*-GaAs Schottky contact. A *n*-GaAs channel was defined by wet etching down to the substrate. 80 nm SiN was deposited over the semiconductor using PECVD at a substrate temperature of 100°C and then lifted off in order to expose the CuGe and FM contacts. Finally, Ti/Au electrodes and bonding pads were fabricated by depositing 25 nm Ti and 120 nm Au by electron beam evaporation.

Measurement. The FMR-spin detection measurement was carried out using a microwave generator, a lock-in amplifier and a current source, as shown in Fig. 1(a). The microwave excitation

signal was coupled to the FM injector through a coaxial cable and an ordinary wire bond. A 120 nm thick Au wire patterned over the FM contact functioned as a stripline, which was terminated at ground. The dc current generating the spin accumulation was fed to the sample using a conventional twisted pair, with one lead connected to one of the ohmic contacts. The differential voltage between a second ohmic reference electrode and the FM contact (connected through a bias tee) was measured using a lock-in amplifier. The microwave signal was modulated using the 100 Hz reference signal of the lock-in amplifier. The circuit therefore measured the difference in the spin accumulation with and without microwave excitation.

---

1. Chappert, C., Fert, A. & Van Dau, F. N. The emergence of spin electronics in data storage. *Nat. Mater.* **6**, 813–823 (2007).
2. Dery, H., Cywiński, L. & Sham, L. J. Spin transference and magnetoresistance amplification in a transistor. *Phys. Rev. B* **73**, 161307 (2006).
3. F. Meier, B. P. Z. (ed.) *Optical Orientation* (North-Holland, Amsterdam, 1984).
4. Jedema, F. J., Heersche, H. B., Filip, A. T., Baselmans, J. J. A. & van Wees, B. J. Electrical detection of spin precession in a metallic mesoscopic spin valve. *Nature* **416**, 713–716 (2002).
5. Lou, X. *et al.* Electrical detection of spin transport in lateral ferromagnet-semiconductor devices. *Nat. Phys.* **3**, 197–202 (2007).
6. Lou, X. *et al.* Electrical detection of spin accumulation at a ferromagnet-semiconductor interface. *Phys. Rev. Lett.* **96**, 176603 (2006).
7. Žutić, I., Fabian, J. & Das Sarma, S. Spintronics: Fundamentals and applications. *Rev. Mod. Phys.* **76**, 323–410 (2004).
8. Dash, S. P., Sharma, S., Patel, R. S., de Jong, M. P. & Jansen, R. Electrical creation of spin polarization in silicon at room temperature. *Nature* **462**, 491–494 (2009).
9. Li, C., van 't Erve, O. & Jonker, B. Electrical injection and detection of spin accumulation in silicon at 500 k with magnetic metal/silicon dioxide contacts. *Nat. Commun.* **2**, 245 (2011).
10. Swartz, A. G. *et al.* Spin-dependent transport across $Co/LaAlO_3/SrTiO_3$ heterojunctions. *Appl. Phys. Lett.* **105**, 032406 (2014).
11. Tinkey, H. N., Li, P. & Appelbaum, I. Inelastic electron tunneling spectroscopy of local "spin accumulation" devices. *Appl. Phys. Lett.* **104**, 232410 (2014).

12. Txoperena, O. *et al.* Impurity-assisted tunneling magnetoresistance under a weak magnetic field. *Phys. Rev. Lett.* **113**, 146601 (2014).

13. Song, Y. & Dery, H. Magnetic-field-modulated resonant tunneling in ferromagnetic-insulator-nonmagnetic junctions. *Phys. Rev. Lett.* **113**, 047205 (2014).

14. Hanbicki, A. T., Jonker, B. T., Itskos, G., Kioseoglou, G. & Petrou, A. Efficient electrical spin injection from a magnetic metal/tunnel barrier contact into a semiconductor. *Appl. Phys. Lett.* **80**, 1240–1242 (2002).

15. Motsnyi, V. F. *et al.* Electrical spin injection in a ferromagnet/tunnel barrier/semiconductor heterostructure. *Appl. Phys. Lett.* **81**, 265–267 (2002).

16. Johnson, M. & Silsbee, R. H. Interfacial charge-spin coupling: Injection and detection of spin magnetization in metals. *Phys. Rev. Lett.* **55**, 1790–1793 (1985).

17. Appelbaum, I., Huang, B. & Monsma, D. J. Electronic measurement and control of spin transport in silicon. *Nature* **447**, 295–298 (2007).

18. Aboelfotoh, M. O., Lin, C. L. & Woodall, J. M. Novel low-resistance ohmic contact to *n*-type GaAs using Cu_3Ge. *Appl. Phys. Lett.* **65**, 3245–3247 (1994).

19. Wang, W. H. *et al.* Magnetic properties and spin polarization of Co_2MnSi heusler alloy thin films epitaxially grown on $GaAs(001)$. *Phys. Rev. B* **71**, 144416 (2005).

20. Akiho, T. *et al.* Electrical injection of spin-polarized electrons and electrical detection of dynamic nuclear polarization using a heusler alloy spin source. *Phys. Rev. B* **87**, 235205 (2013).

21. Saito, T., Tezuka, N., Matsuura, M. & Sugimoto, S. Spin injection, transport, and detection at room temperature in a lateral spin transport device with $Co_2FeAl_{0.5}Si_{0.5}/n-GaAs$ schottky tunnel junctions. *Appl. Phys. Express* **6**, 103006 (2013).

22. Rashba, E. I. Theory of electrical spin injection: Tunnel contacts as a solution of the conductivity mismatch problem. *Phys. Rev. B* **62**, R16267–R16270 (2000).

23. Schmidt, G., Ferrand, D., Molenkamp, L. W., Filip, A. T. & van Wees, B. J. Fundamental obstacle for electrical spin injection from a ferromagnetic metal into a diffusive semiconductor. *Phys. Rev. B* **62**, R4790–R4793 (2000).

24. Stephens, J. *et al.* Spin accumulation in forward-biased $MnAs/GaAs$ schottky diodes. *Phys. Rev. Lett.* **93**, 097602 (2004).

25. Kittel, C. On the theory of ferromagnetic resonance absorption. *Phys. Rev.* **73**, 155–161 (1948).

26. Sharma, B. (ed.) *Metal-Semiconductor Schottky Barrier Junctions and Their Applications* (Springer,

1984).

27. Liu, C. *et al.* Electrical detection of ferromagnetic resonance in ferromagnet/$n-$GaAs heterostructures by tunneling anisotropic magnetoresistance. *Appl. Phys. Lett.* **105**, 212401 (2014).
28. Moser, J. *et al.* Tunneling anisotropic magnetoresistance and spin-orbit coupling in Fe/GaAs/Au tunnel junctions. *Phys. Rev. Lett.* **99**, 056601 (2007).
29. Kato, Y. K., Myers, R. C., Gossard, A. C. & Awschalom, D. D. Observation of the spin hall effect in semiconductors. *Science* **306**, 1910–1913 (2004).
30. Furis, M., Smith, D. L., Crooker, S. A. & Reno, J. L. Bias-dependent electron spin lifetimes in $n-$GaAs and the role of donor impact ionization. *Appl. Phys. Lett.* **89**, 102102 (2006).
31. Crooker, S. A. *et al.* Bias-controlled sensitivity of ferromagnet/semiconductor electrical spin detectors. *Phys. Rev. B* **80**, 041305 (2009).
32. Chan, M. K. *et al.* Hyperfine interactions and spin transport in ferromagnet-semiconductor heterostructures. *Phys. Rev. B* **80**, 161206 (2009).
33. Lau, W. H., Olesberg, J. T. & Flatté, M. E. Electron-spin decoherence in bulk and quantum-well zinc-blende semiconductors. *Phys. Rev. B* **64**, 161301 (2001).

Acknowledgments

This work was supported by the National Science Foundation (NSF) under DMR-1104951, C-SPIN, one of the six centers of STARnet, a SRC program sponsored by MARCO and DARPA, the Materials Research Science and Engineering Centers (MRSEC) program of NSF under DMR 08-19885, and the NSF NNIN program.

Author contributions

C.L. fabricated the FMR devices, performed the FMR-spin detection experiment, developed the theoretical model and wrote the paper with P.A.C.. S.J.P. grew all the FM/n-GaAs heterostructures used in this work. T.A.P. fabricated the non-local spin valve devices and took the non-local spin valve measurement. C.C.G. and K.D.C. took the non-local Hanle measurement. G.S. took some of the TAMR measurements. C.C.G. developed software for performing the experiment and analyzing the data. P.A.C. provided the initial concept, and P.A.C. and C.J.P. supervised the project.

Additional information

Competing financial interests: The authors declare no competing financial interests.